Light Extraction with Dielectric Nanoantenna Arrays

Giovanni Pellegrini,* Giovanni Mattei, and Paolo Mazzoldi

CNISM, Department of Physics, University of Padova, Via Marzolo 8, 35131 Padova, Italy

ABSTRACT SiO_2 and TiO_2 dielectric nanoparticles are arranged in linear arrays, supporting collective Bragg modes, and employed as dielectric nanoantennae. Electrodynamic calculations show that strong, tunable, and lossless light extraction is obtained in a wide spectral range, including UV, visible, and near-infrared regions, in opposition to poor enhancement features of isolated dielectric nanoparticles. Emission quantum efficiencies comparable to those obtained employing metallic structures are achieved, with strong emission enhancement even for poor emitter position and dipole moment orientation.

KEYWORDS: fluorescence enhancement · nanoantenna · plasmon · plasmonic crystal · photonic crystal

Plasmonic metallic nanoantennae are receiving steadily growing attention for their ability to tailor the light emission properties of nearby emitting structures such as molecules or quantum dots (QDs).[1−4] Metal nanoantennae are able to modify the angular distribution of the emitted radiation and to dramatically enhance the emission quantum efficiency.[5−8] Furthermore, it has recently been demonstrated that multiple particle nanoantennae may be employed as efficient polarization rotators.[9] The main reason of these outstanding light manipulation performances resides in a metal nanoparticle (NP) large scattering cross section, with emitted photons strongly coupling to the plasmonic modes supported by the nanoantenna.[10,11] On the other hand, dielectric nanoantennae have poor light extraction properties overall, mainly assignable to their small scattering cross section, though the use of a dielectric NP could prove attractive for the absence of ohmic losses in the light extraction process.[12] Very recently, a great deal of interest was attracted by the ultra-narrow collective resonances supported by regular arrays of metallic NPs, as it has also been shown, both theoretically and experimentally, that these resonances may be exploited for superior and tunable light extraction performances.[13−18]

In the following, a multiple scattering technique (*i.e.*, generalized multiparticle Mie (GMM) theory) is used to study, at first, a single emitter coupled to an isolated dielectric NP, then this unit cell is repeated in space to form a linear array.[19−21] The influence on emitted radiation is studied as a function of antenna structural and compositional variables such as cell parameter and NP size and material. Finally, the effect of emitter position and orientation is taken into account to exhaustively assess the nanoantenna features. A typical sketch of the employed array structures is seen in Figure 1, with the isolated unit placed at the origin and highlighted by the blue box.

In our theoretical framework, the emitter is modeled as a classical dipole with intrinsic quantum efficiency $q_o = \gamma_r^o/(\gamma_r^o + \gamma_{nr}^o)$, where γ_r^o and γ_{nr}^o are the radiative and nonradiative recombination rates of the isolated emitter. The influence of the antenna on the emission processes is easily expressed in terms of power dissipated inside the nanoantenna and radiated by the nanoantenna emitter ensemble. Normalized modified rates are then expressed as $\gamma_r/\gamma_r^o = P_r/P_r^o$ and $\gamma_{abs}/\gamma_r^o = P_{abs}/P_r^o$, with γ_{abs} being the contribution to nonradiative recombination rates related to the power dissipated inside the nanoantenna, P_{abs}, P_r the power radiated by the emitter−antenna system, and P_r^o the power radiated by a classical dipole.[10,22] By writing the overall nonradiative rate as $\gamma_{nr} = \gamma_{nr}^o + \gamma_{abs}$, we may finally express the modified quantum efficiency q in the general case:[4,22,23]

$$q = \frac{\gamma_r/\gamma_r^o}{\gamma_r/\gamma_r^o + \gamma_{abs}/\gamma_r^o + (1 - q_o)/q_o} \quad (1)$$

*Address correspondence to pellegrini@padova.infm.it.

Received for review May 11, 2009 and accepted July 28, 2009.

Published online August 3, 2009.
10.1021/nn900481v CCC: $40.75

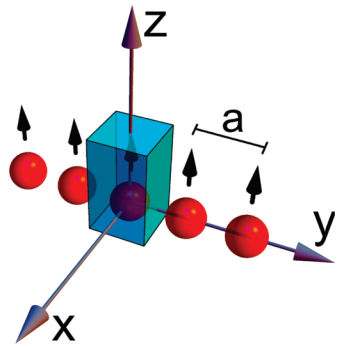

Figure 1. Sketch of typical nanoantenna array configuration. Array principal axis is always *y*-oriented, with cell parameter *a*. Dipoles are always *z*-oriented, if not otherwise indicated, 5 nm above the sphere surface. The typical isolated antenna unit is highlighted in the blue box.

RESULTS AND DISCUSSION

Figure 2b shows the γ_r/γ_r^o and γ_{abs}/γ_r^o spectra for a *z*-oriented dipole placed 5 nm away from a SiO_2 sphere, with radii ranging from 50 to 150 nm. Extremely small enhancement of the radiative recombination rates is observed from the ultraviolet (UV) to the near-infrared (NIR) range ($\gamma_r/\gamma_r^o \sim 2.5$), with enhancement maxima red shifting as the size of the antenna increases.[12] Likewise, no substantial power dissipation inside the nanoantenna is seen, in agreement with what should be expected by a quick analysis of SiO_2 optical constants in the observed wavelength range (Figure 2a). Absence of ohmic losses is a desirable feature, in order to avoid the introduction of new nonradiative channels. Spectra for rutile TiO_2 nanoantennae are reported in Figure 2c. Slightly larger enhancements of the radiative recombination rates are observed ($\gamma_r/\gamma_r^o \sim 10$), with sharp peaks likely assignable to low-order whispering gallery modes (WGMs),[24,25] dominating the spectrum at higher energies. Since these modes are not the main subject of the present paper, we limit ourselves to notice that radiative rate enhancements of more than 1 order of magnitude are seen, making them promising for light extraction applications. Dipolar scattering maxima are present at lower energies and follow the behavior already observed in SiO_2 NPs. No power dissipation inside the nanoantenna is observed for wavelengths above 350 nm, becoming significant for wavelengths in the UV range, where TiO_2 begins to show a dispersive behavior (Figure 2a).

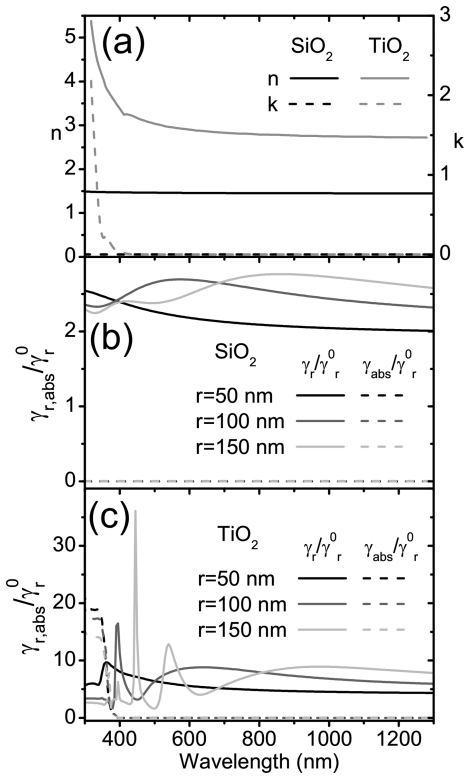

Figure 2. (a) SiO_2 and TiO_2 complex optical constants. Normalized radiative and nonradiative recombination rate curves for an emitter coupled to SiO_2 (b) and TiO_2 (c) spheres in vacuum. Particle emitter distance is 5 nm.

In the following, Bragg resonances supported by regular arrays of nanoparticles are employed to boost the light extraction characteristics of dielectric nanoantennae which otherwise, with the exception of WGMs, would be unable to efficiently enhance light emission processes as just shown. In this framework, GMM theory is applied to study regular arrays of the antenna emitter units described above. Linear chains are chosen to be 1000 units long in order to fully develop the geometric resonances. All of the structures are taken to be in vacuum, and their optical constants are obtained from the literature.[26] The chain cell parameter *a*, defined as the center to center antenna distance, varies from 250 to 1200 nm in 50 nm steps, with particle emitters separation kept fixed at 5 nm. Up to 80 multipoles have been included in the calculations in order to ensure spectral convergence at all the computed wavelengths.

Figure 3 reports radiative rate enhancement spectra for SiO_2 nanoantenna arrays based upon the isolated unit adopted before. Antenna contributions to the nonradiative recombination rate (γ_{abs}) are always negligible at the resonance wavelengths of interest, as can be argued from Figure 2, and are therefore omitted. Without entering the physical details of Bragg resonances, which have been discussed thoroughly elsewhere,[18,27−29] we limit ourselves to notice that, in vacuum, sharp radiative enhancement peaks show up at roughly $\lambda \sim a/m$, where *m* is an integer and *a* is the cell parameter. This behavior is easily understood if we describe our system in the coupled dipole theoretical framework and the nanoantennae by the effective polarizability $\alpha_{eff} = \alpha/(1 - \alpha S)$, with *S* the retarded dipole sum and α the original antenna polarizability: scattering resonances arises whenever $\mathrm{Re}[\alpha^{-1}] \sim \mathrm{Re}[S]$, that is, at $\lambda \sim a/m$, with narrow resonance shapes determined by both singularities in Re[*S*] and partial cancellations between Im[*S*] and radiative damping terms.[27−29] The ratio γ_r/γ_r^o reaches values as high as 50 in the $r = 150$ nm best performing structures when the collective resonances are located around the scattering maximum of

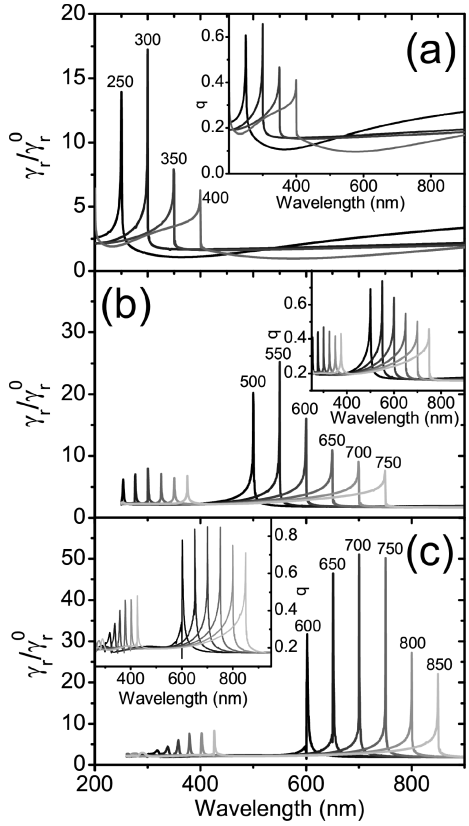

Figure 3. Normalized radiative recombination rate curves for an emitter coupled to a SiO_2 nanoantenna array: (a) r = 50 nm, (b) r = 100 nm, (c) r = 150 nm: peaks are labeled with the respective array pitch expressed in nm. Insets: corresponding q *vs* λ spectra for an emitter with an intrinsic q_0 = 0.1 quantum efficiency. Particle emitter distance is 5 nm.

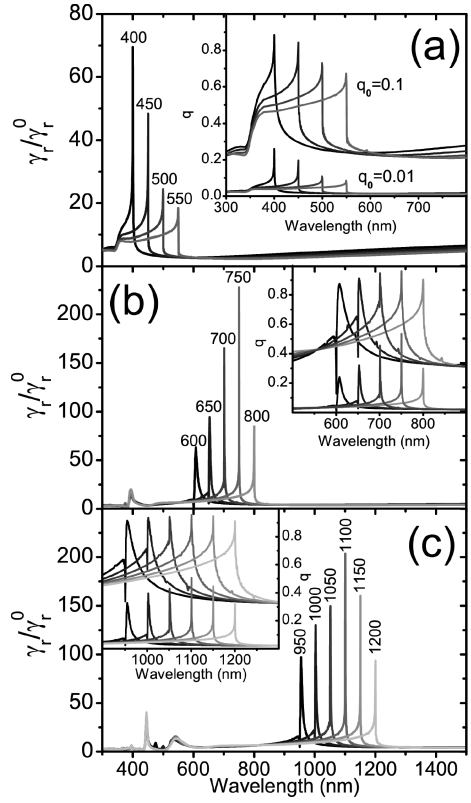

Figure 4. Normalized radiative recombination rate curves for an emitter coupled to a TiO_2 nanoantenna array: (a) r = 50 nm, (b) r = 100 nm, (c) r = 150 nm: peaks are labeled with the respective array pitch expressed in nm. Insets: corresponding q *vs* λ spectra for an emitter with an intrinsic q_0 = 0.1 (upper curve set) and q_0 = 0.01 (lower curve set) quantum efficiency. Particle emitter distance is 5 nm.

the isolated nanoantenna, as in the metallic sphere case.[18] Better emission performances are obtained for larger antennae in the red and NIR ranges: this trend is most likely assignable to an overall beneficial trade-off between larger scattering cross sections for bigger antenna sizes, against a worse emitter antenna coupling.[4] We finally notice that for r = 100 and 150 nm nanoantennae, weaker second-order resonances are visible in the blue and UV ranges, where SiO_2 still shows a lossless behavior. In the insets, q *versus* λ spectra are presented. A q_0 = 0.1 emitter is chosen, with obtained final efficiencies as high as q = 0.8 in the best performing case and above q = 0.5 for a wide range of parameters. It is worth noting that in this case selective enhancement is still possible even for an emitter with a relatively high initial quantum yield since dielectric nanoantennae are essentially unable to provide light extraction in Bragg off-resonance conditions, which is not the case for metallic nanoparticles.[18]

TiO_2 nanoantenna arrays (Figure 4) show a qualitatively similar behavior but differ significantly in the resonance strength. Radiative rate enhancements larger than 2 orders of magnitude are observed, where best performances are again found for the structures based on larger antennae in the red and NIR ranges. Collective resonances are red-shifted with respect to the SiO_2 situation, in agreement with the position of single particle dipolar scattering. Second-order resonances are still present at shorter wavelengths, though not visible at the present plot scale, given their superimposition with the WGMs. Modification of emitter quantum efficiency is reported in the insets in Figure 4. If a q_0 = 0.1 emitter is chosen, remarkable final $q > 0.9$ efficiencies are obtained, while q = 0.6 peak efficiencies are found if a worse q_0 = 0.01 is adopted, with performances comparable to those of metallic nanoantennae.[11,18] In all of the above examples, Bragg resonance tuning is obtained by variation of structural parameters such as cell parameter a and sphere radius; nevertheless, resonance tuning by changing the matrix refractive index may still be obtained, keeping in mind the obvious limitations imposed by the nanoantenna refractive index.[18]

We remark that, in our theoretical framework, emitters are modeled as coherently oscillating dipoles. This assumption may be retained as reasonable since collective spontaneous emission has been theoretically predicted for linear arrays of N two-states atoms, and cooperative spontaneous emission has been observed for both QDs or ion ensembles.[30−33] Furthermore, it has

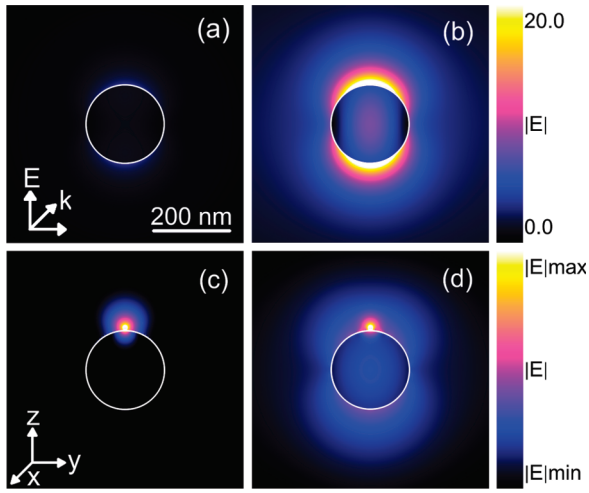

Figure 5. Local-field plots for best performing TiO_2 nanoantenna array, $r = 100$ nm, $a = 750$ nm, and corresponding isolated unit, at $\lambda = 750$ nm. A logarithmic scale is adopted for dipole−antenna field plots in (c) and (d), with 3 orders of magnitude between $|\mathbf{E}|_{max}$ and $|\mathbf{E}|_{min}$. (a) Isolated unit, unitary amplitude plane wave illumination, (b) array, unitary amplitude plane wave illumination, (c) isolated unit, *z*-oriented dipole illumination, (d) array, *z*-oriented dipole illumination. Particle emitter distance is 5 nm. Antenna is highlighted by the thin white line.

been recently experimentally demonstrated that Bragg resonances supported by plasmonic crystals are able to enhance the emission of organic chromophores in a tunable and directional fashion.[17]

The investigated dielectric nanoantennae are interesting not only for their far-field properties but also for their near-field ones; therefore, as a next step, we focus on a single nanoantenna array at a fixed wavelength, that is, on the best performing $r = 100$ nm, $a = 750$ nm TiO_2 linear chain coupled to the worse $q_0 = 0.01$ emitter. We shall first tackle the array local-field features then switch to the study of light extraction performances as a function of emitter position and dipole moment orientation.

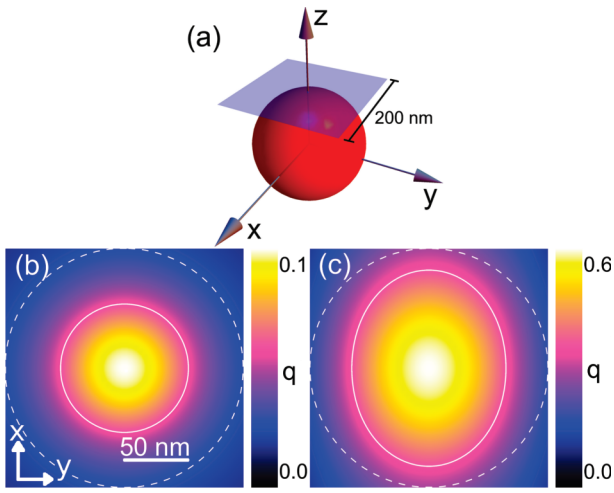

Figure 6. Efficiency enhancement position mapping for best performing TiO_2 nanoantenna array, $r = 100$ nm, $a = 750$ nm, and corresponding isolated unit, at $\lambda = 750$ nm. A $q_0 = 0.01$ *z*-oriented, *z*-centered dipole moving on a *xy* plane, 5 nm above the sphere surface is adopted: (a) plotting plane, (b) isolated unit, (c) array. White closed lines are half intensity level curves, and dashed lines are the antenna in-plane projection.

Figure 5a reports local-field plots for an isolated unit of the best performing array, illuminated by a monochromatic, unit amplitude plane wave at $\lambda = 750$ nm. A small field enhancement is seen, as might been expected from the poor light extraction properties observed before (Figure 2c). Likewise, the local-field of the single antenna−dipole unit (Figure 5c) shows a poor antenna emitter coupling, with essentially no emission enhancement induced by the presence of the dielectric nanocluster. Much larger local-field enhancements are obtained if the same plane wave illuminates the nanoantennae arranged as a linear chain. Field enhancements as high as $|\mathbf{E}| \sim 20$, comparable to the ones of isolated metallic nanoparticles, are seen, which of course calls for much more prominent light extraction performances.[11] This is clearly seen in Figure 5d, which reports the field map for the antenna−dipole array. Excellent emitter antenna coupling and strong emission enhancement are clearly visible. Furthermore, we notice that the field distribution reveals the purely dipolar nature of the Bragg resonance.

As a further issue, we investigated the light extraction properties of the best performing array, as the emitter is displaced on a 200 nm side *xy* plane, 5 nm above the surface of an isolated $r = 100$ nm TiO_2 nanoantenna (Figure 6a). Figure 6b reports a quantum efficiency mapping for a *z*-oriented, $q_0 = 0.01$, 750 nm emitting dipole: overall extraction efficiency is poor, as already noticed, with maximum emission for the dipole placed directly at the nanoantenna zenith. Efficiency mapping exhibits a cylindrical symmetry as expected. Light extraction weakens as the dipole moves away from the *z* axis, with an efficiency peak fwhm of about ~110 nm. The same kind of mapping is performed for the whole best performing array. Figure 6c shows that peak $q \sim 0.6$ extraction is again obtained for an emitter placed exactly on the *z* axis. Cylindrical symmetry is broken by the arrangement of the nanoantennae in a regular array, with emission enhancement dropping more slowly if the dipole is displaced along the *x* direction, normally to the chain principal axis.[18,34] Nevertheless, both *x* and *y* fwhm, being about ~180 and 130 nm, respectively, are larger than in the single nanoantenna case. The reason for the slower emission decay for the *x* displacement is easily understood if a simplified dipole chain model is considered; in this case, (i) the Bragg resonances are supported only if the dipole orientation is not parallel to the chain principal axis,[27,34] and (ii) the strength of the resonance is proportional to the dipole projection on a plane normal to the chain axis. Therefore, if the emitter is displaced in the *x* direction, it is clear from simple symmetry considerations that the dipole moment induced by the emitter on the nanoantenna has no axial component and entirely concurs to the formation of the Bragg resonance. This of course

shall not be the case if the emitter is moved along the array principal axis.

Finally, we turn our attention to the dependence of recombination rate and quantum efficiency enhancement as a function of the dipole orientation with respect to the antenna.[4] As done before, we shall treat first the isolated nanoantenna and then the array case, where all of the relevant parameters are taken to be the same as the best performing structure. Orientation-dependent quantum efficiency enhancement is studied at four different dipole positions, as shown in Figure 7a. Figure 7b shows *q versus* orientation polar surface plots for emitters in the four configurations. We first notice that all of the quantum efficiency surfaces are described by specific dumbbell-like shapes, with better light extraction features always found for orientations normal to the antenna surface. In the case of the isolated sphere, efficiency enhancement surfaces for dipole placed in positions (i) and (iv) correspond to the best and worst performing case, respectively, with shapes for emitters in positions (ii) and (iii) being identical except for a $\pi/2$ rotation. Dumbbell-shaped efficiency surface plots may be explained by invoking Green's dyadic symmetry properties. It has been indeed recently demonstrated that emission *versus* dipole orientation behavior can be fully described by three principal orthogonal axis and the corresponding recombination rates.[35] Recombination rate and quantum efficiency enhancement in an arbitrary orientation are a function of the three principal rates and, in particular, a quadric defined on the unit sphere. Only specific surfaces are allowed, being classified by the relative ratios of the principal recombination rates.[35] In this framework, dumbbell-shaped enhancement surfaces are easily understood. From a simple symmetry analysis, it is clear that, for the system under consideration, one of the principal dipole axes is normal to the sphere surface while the other two, which of course are degenerate, lie on the corresponding tangential plane. Better emission enhancement is always found for dipole normal orientation since the dipole moment induced on the antenna by the emitter is larger in this configuration.[4] Enhancement surfaces for the best performing array at $\lambda = 750$ nm are shown in Figure 7c. As in the previous case, efficiency surfaces are dumbbell-shaped, without the tangential plane degeneracy which is lifted by the linear arrangement. Surface plots exhibit the most general enhancement shape, which is clearly seen for the emitters placed in positions (ii) and (iii).[35] Best and worst light extractions are again for normal and parallel dipole orientation and positions (i) and (iv), respectively. Enhancement shapes for positions (ii) and (iii) are now different, with better light extraction in the latter case, in agreement with the results for the position mapping. Furthermore, comparing isolated and array nanoantennae, we notice that array efficiency surfaces show less elongated shapes than the single

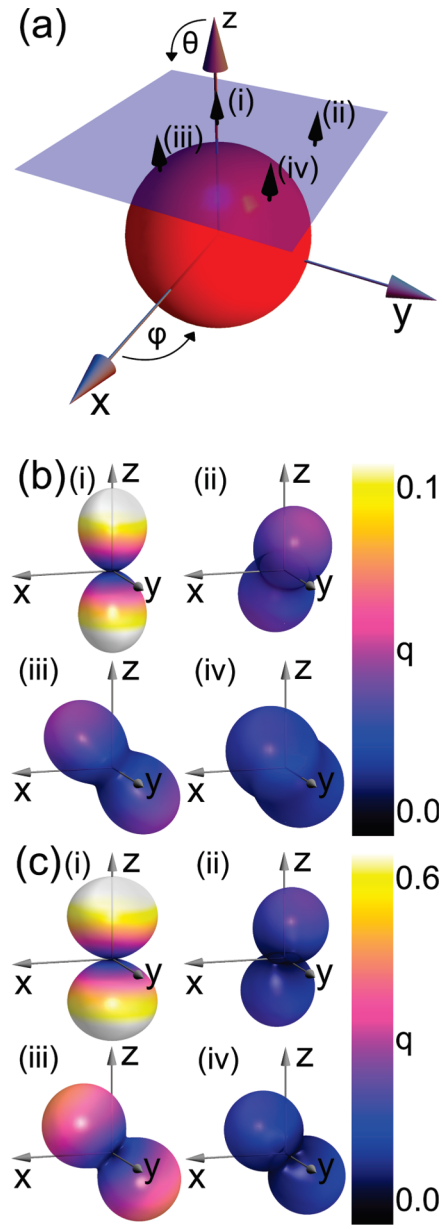

Figure 7. Polar surface plots representing the dipole orientation quantum efficiency enhancement dependence in real space. Emitters are in four positions on a *xy* plane, 5 nm above the sphere surface ($z = 105$ nm plane): (i) $\mathbf{r} = (0,0,105)$ nm, (ii) $\mathbf{r} = (0,105,105)$ nm, (ii) $\mathbf{r} = (105,0,105)$ nm, (iv) $\mathbf{r} = (105,105,105)$ nm, with the antenna placed at the origin. Best performing TiO_2 nanoantenna array ($r = 100$ nm, $a = 750$ nm), corresponding isolated unit, and a $q_0 = 0.01$ dipole emitting at $\lambda = 750$ nm are adopted. (a) Dipole positions; (b) isolated unit efficiency enhancement surfaces; (c) array efficiency enhancement surfaces.

antenna case, which in turn means that nanoantenna arrays tolerate much larger angular deviation from the best performing dipole orientation, with efficiency loss of about 30% for $\theta = \pi/4$ tiltings.

As a closing remark, we stress that dielectric nanoantenna arrays retain all of the directional emission properties exhibited by plasmonic arrays, these being only determined by the antenna geometrical arrangement and isolated unit emission pattern.[18,34]

CONCLUSIONS

In summary we have demonstrated, by multiple scattering calculations, strong recombination rate and quantum efficiency enhancement by dielectric nanoantenna arrays. While isolated dielectric nanoparticles show extremely poor nanoantenna properties, regular arrays supporting Bragg modes are able to provide strong, tunable, directional, and wavelength selective light extraction, which is normally considered as peculiar of metallic nanoantennae. Lossless emission enhancement is obtained in a wide spectral range, from the UV for SiO_2 structures to the NIR for TiO_2 arrays. Selective light extraction is also obtained for emitter with a relatively high initial quantum efficiency ($q_0 \sim 0.1$) since no significant recombination rate enhancement is achieved in Bragg off-resonance conditions. Arrays overperform isolated nanoantennae for more subtle yet fundamental features; that is, periodic structures provide high emission efficiencies even for poor emitter placement and dipole moment orientation. Finally, we stress that typical dielectric antenna dimensions, from 100 to 400 nm in diameter, make their realization readily achievable with common lithographic and nanoimprinting techniques or by standard colloidal chemistry synthesis of dielectric nanoparticles,[36] making them particularly attractive for practical applications.[37,38]

The obtained results might find important application in the realization of a large variety of photonic, lighting, and sensing devices.[6,17,39−43]

METHODS

A multiple scattering approach (*i.e.*, generalized multiparticle Mie theory) has been employed for all theoretical calculations:[19] software has been developed from scratch, following closely the guidelines provided by Xu and Mackowski for the numerical implementation.[19,44−47]

Model systems consist of 1000 sphere long linear chains, with a corresponding dipole emitter for each sphere. Dipoles are modeled as pure sources of the incident field; that is, they are not driven by the field of the other dipoles and by the field scattered by the antennae. This corresponds to an experimental setup where a Stokes shift between excitation and emission exists.[17,48]

Power radiated by the antenna emitter ensemble and power dissipated inside the nanoantennae are calculated by analytical and numerical integration of the Poynting vector over the appropriate surfaces, and the results are then cross-checked.

Optical constants come from experimental data sets and are obtained in tabulated form from the literature.[26] They are then interpolated with standard procedures for the practical calculations.

REFERENCES AND NOTES

1. Mertens, H.; Biteen, J. S.; Atwater, H. A.; Polman, A. Polarization-Selective Plasmon-Enhanced Silicon Quantum-Dot Luminescence. *Nano Lett.* **2006**, *6*, 2622–2625.
2. Biteen, J. S.; Lewis, N. S.; Atwater, H. A.; Mertens, H.; Polman, A. Spectral Tuning of Plasmon-Enhanced Silicon Quantum Dot Luminescence. *Appl. Phys. Lett.* **2006**, *88*, 131109.
3. Biteen, J. S.; Sweatlock, L. A.; Mertens, H.; Lewis, N. S.; Polman, A.; Atwater, H. A. Plasmon-Enhanced Photoluminescence of Silicon Quantum Dots: Simulation and Experiment. *J. Phys. Chem. C* **2007**, *111*, 13372–13377.
4. Mertens, H.; Koenderink, A. F.; Polman, A. Plasmon-Enhanced Luminescence Near Noble-Metal Nanospheres: Comparison of Exact Theory and an Improved Gersten and Nitzan Model. *Phys. Rev. B* **2007**, *76*, 115123.
5. Anger, P.; Bharadwaj, P.; Novotny, L. Enhancement and Quenching of Single Molecule Fluorescence. *Phys. Rev. Lett.* **2006**, *96*, 113002.
6. Mertens, H.; Polman, A. Plasmon-Enhanced Erbium Luminescence. *Appl. Phys. Lett.* **2006**, *89*, 211107.
7. Muskens, O. L.; Giannini, V.; Sánchez-Gil, J. A.; J, G. R. Strong Enhancement of the Radiative Decay Rate of Emitters by Single Plasmonic Nanoantennas. *Nano Lett.* **2007**, *7*, 2871–2875.
8. Taminiau, T. H.; Stefani, F. D.; Segerink, F. B.; van Hulst, N. F. Optical Antennas Direct Single-Molecule Emission. *Nat. Photon.* **2008**, *2*, 234–237.
9. Li, Z.; Shegai, T.; Haran, G.; Xu, H. Multiple-Particle Nanoantennas for Enormous Enhancement and Polarization Control of Light Emission. *ACS Nano* **2009**, *3*, 637–642.
10. Ruppin, R. Decay of an Excited Molecule near a Small Metal Sphere. *J. Chem. Phys.* **1982**, *76*, 1681–1684.
11. Rogobete, L.; Kaminski, F.; Agio, M.; Sandoghdar, V. Design of Plasmonic Nanoantennae for Enhancing Spontaneous Emission. *Opt. Lett.* **2007**, *32*, 1623.
12. Bohren, C.; Huffman, D. *Absorption and Scattering of Light by Small Particles*; Wiley-Interscience: New York, 1998.
13. Auguie, B.; Barnes, W. L. Collective Resonances in Gold Nanoparticle Arrays. *Phys. Rev. Lett.* **2008**, *101*, 143902.
14. Kravets, V. G.; Schedin, F.; Grigorenko, A. N. Extremely Narrow Plasmon Resonances Based on Diffraction Coupling of Localized Plasmons in Arrays of Metallic Nanoparticles. *Phys. Rev. Lett.* **2008**, *101*, 087403.
15. Chu, Y.; Schonbrun, E.; Yang, T.; Crozier, K. B. Experimental Observation of Narrow Surface Plasmon Resonances in Gold Nanoparticle Arrays. *Appl. Phys. Lett.* **2008**, *93*, 181108.
16. Auguié, B.; Barnes, W. L. Diffractive Coupling in Gold Nanoparticle Arrays and the Effect of Disorder. *Opt. Lett.* **2009**, *34*, 401–403.
17. Vecchi, G.; Giannini, V.; Rivas, J. G. Shaping the Fluorescent Emission by Lattice Resonances in Plasmonic Crystals of Nanoantennas. *Phys. Rev. Lett.* **2009**, *102*, 146807.
18. Pellegrini, G.; Mattei, G.; Mazzoldi, P. Tunable, Directional and Wavelength Selective Plasmonic Nanoantenna Arrays. *Nanotechnology* **2009**, 065201.
19. Xu, Y. L. *Appl. Opt.* **1995**, *34*, 4573.
20. Pellegrini, G.; Mattei, G.; Bello, V.; Mazzoldi, P. Interacting Metal Nanoparticles: Optical Properties from Nanoparticle Dimers to Core-Satellite Systems. *Mater. Sci. Eng., C* **2007**, *27*, 1347–1350.
21. Pellegrini, G.; Bello, V.; Mattei, G.; Mazzoldi, P. Local-Field Enhancement and Plasmon Tuning in Bimetallic Nanoplanets. *Opt. Express* **2007**, *15*, 10097–10102.
22. Bharadwaj, P.; Novotny, L. Spectral Dependence of Single Molecule Fluorescence Enhancement. *Opt. Express* **2007**, *15*, 14266.
23. Ringler, M.; Schwemer, A.; Wunderlich, M.; Nichtl, A.; Kurzinger, K.; Klar, T. A.; Feldmann, J. Shaping Emission Spectra of Fluorescent Molecules with Single Plasmonic Nanoresonators. *Phys. Rev. Lett.* **2008**, *100*, 203002.
24. Cole, R. M.; Sugawara, Y.; Baumberg, J. J.; Mahajan, S.; Abdelsalam, M.; Bartlett, P. N. Easily Coupled Whispering Gallery Plasmons in Dielectric Nanospheres Embedded in Gold Films. *Phys. Rev. Lett.* **2006**, *97*, 137401.

25. Dantham, V. R.; Bisht, P. B. High-Q Whispering Gallery Modes of Doped and Coated Single Microspheres and Their Effect on Radiative Rate. *J. Opt. Soc. Am. B* **2009**, *26*, 290–300.
26. Palik, E. D. *Handbook of Optical Constants of Solids*; Academic Press: New York, 1985.
27. Zou, S. L.; Schatz, G. C. Narrow Plasmonic/Photonic Extinction and Scattering Line Shapes for One and Two Dimensional Silver Nanoparticle Arrays. *J. Chem. Phys.* **2006**, *121*, 12606–12612.
28. Zou, S. L.; Janel, N.; Schatz, G. C. Silver Nanoparticle Array Structures that Produce Remarkably Narrow Plasmon Lineshapes. *J. Chem. Phys.* **2004**, *120*, 10871–10875.
29. Zou, S. L.; Schatz, G. C. Response to Comment on "Silver Nanoparticle Array Structures that Produce Remarkable Narrow Plasmon Line Shapes". *J. Chem. Phys.* **2006**, *122*, 097102.
30. Clemens, J. P.; Horvath, L.; Sanders, B. C.; Carmichael, H. J. Collective Spontaneous Emission from a Line of Atoms. *Phys. Rev. A* **2003**, *68*, 023809.
31. DeVoe, R. G.; Brewer, R. G. Observation of Superradiant and Subradiant Spontaneous Emission of Two Trapped Ions. *Phys. Rev. Lett.* **1996**, *76*, 2049–2052.
32. Scheibner, M.; Schmidt, T.; Worschech, L.; Forchel, A.; Bacher, G.; Passow, T.; Hommel, D. Superradiance of Quantum Dots. *Nat. Phys.* **2007**, *3*, 106–110.
33. Dahmen, C.; Schmidt, B.; vonPlessen, G. Radiation Damping in Metal Nanoparticle Pairs. *Nano Lett.* **2007**, *7*, 318–322.
34. Silver, S. *Microwave Antenna Theory and Design*; Institution of Electrical Engineers, 1984.
35. VosW. L. KoenderinkA. F. Nikolaevl. S. Strong Dependence of the Optical Emission Rates of a Two-Level Quantum Emitter in any Nanophotonic Environment on the Orientation of the Transition Dipole Moment; arXiv.org e-Print archive, 2009 arXiv:0902.1862v1
36. Stober, W.; Fink, A.; Bohn, E. Controlled Growth of Monodisperse Silica Spheres in the Micron Size Range. *J. Colloid Interface Sci.* **1968**, *26*, 62–69.
37. Tormen, M.; Carpentiero, A.; Ferrari, E.; Cojoc, D.; Fabrizio, E. D. Novel Fabrication Method for Three-Dimensional Nanostructuring: an Application to Micro-Optics. *Nanotechnology* **2007**, *18*, 385301.
38. Ormonde, A. D.; Hicks, E. C. M.; Castillo, J.; Duyne, R. P. V. Nanosphere Lithography: Fabrication of Large-Area Ag Nanoparticle Arrays by Convective Self-Assembly and Their Characterization by Scanning UV−Visible Extinction Spectroscopy. *Langmuir* **2004**, *20*, 6927–6931.
39. Tam, F.; Goodrich, G. P.; Johnson, B. R.; Halas, N. J. Plasmonic Enhancement of Molecular Fluorescence. *Nano Lett.* **2007**, *7*, 496–501.
40. Haes, A. J.; Duyne, R. P. V. A Nanoscale Optical Biosensor: Sensitivity and Selectivity of an Approach Based on the Localized Surface Plasmon Resonance Spectroscopy of Triangular Silver Nanoparticles. *J. Am. Chem. Soc.* **2002**, *124*, 10596–10604.
41. Haes, A. J.; Zou, S.; Schatz, G. C.; Duyne, R. P. V. A Nanoscale Optical Biosensor: The Long Range Distance Dependence of the Localized Surface Plasmon Resonance of Noble Metal Nanoparticles. *J. Phys. Chem. B* **2004**, *108*, 109–116.
42. Okamoto, K.; Niki, I.; Shvartser, A.; Narukawa, Y.; Mukai, T.; Scherer, A. Surface-Plasmon-Enhanced Light Emitters Based on InGaN Quantum Wells. *Nat. Mater.* **2004**, *3*, 601–605.
43. Tvingstedt, K.; Zilio, S. D.; Inganäs, O.; Tormen, M. Trapping Light with Micro Lenses in Thin Film Organic Photovoltaic Cells. *Opt. Express* **2008**, *16*, 21608–21615.
44. Xu, Y. L. Fast Evaluation of the Gaunt Coefficients. *Math. Comput.* **1996**, *65*, 1601–1612.
45. Xu, Y. L. Electromagnetic Scattering by an Aggregate of Spheres: Far Field. *Appl. Opt.* **1997**, *36*, 9496–9508.
46. Xu, Y. L. Efficient Evaluation of Vector Translation Coefficients in Multiparticle Light-Scattering Theories. *J. Comput. Phys.* **1998**, *139*, 137–165.
47. Mackowski, D. W. Analysis of Radiative Scattering for Multiple Sphere Configurations. *Proc. R. Soc. London, Ser. A* **1991**, *433*, 599–614.
48. Gerber, S.; Reil, F.; Hohenester, U.; Schlagenhaufen, T.; Krenn, J. R.; Leitner, A. Tailoring Light Emission Properties of Fluorophores by Coupling to Resonance-Tuned Metallic Nanostructures. *Phys. Rev. B* **2007**, *75*, 073404.